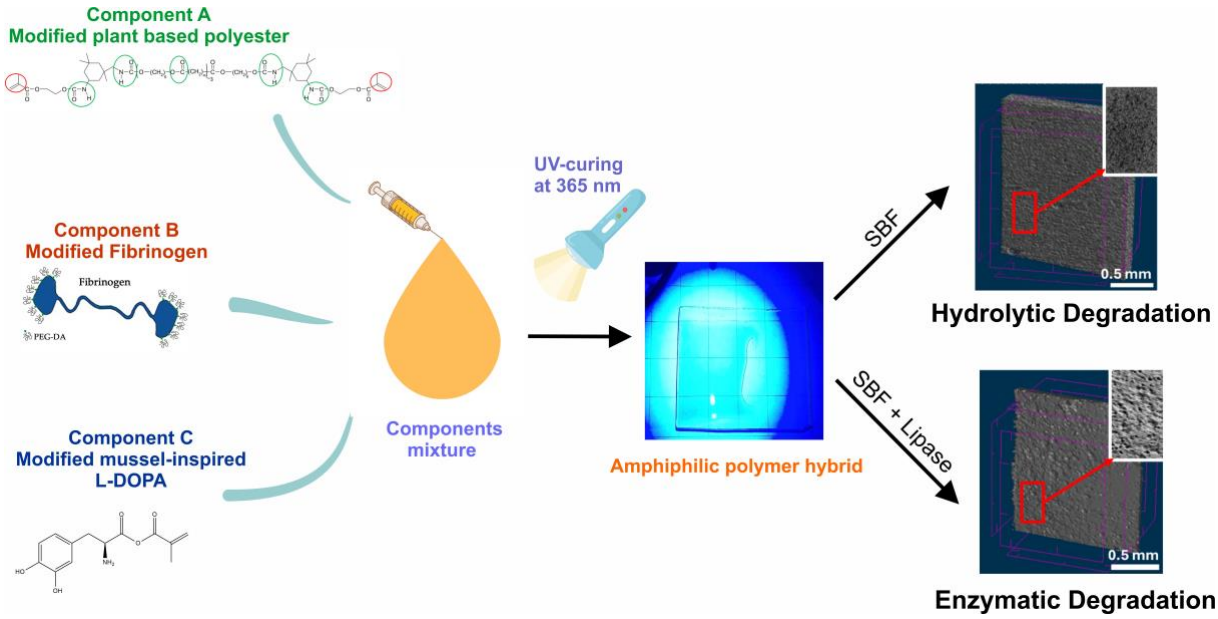

Hydrolytic and Enzymatic Degradation of Photocurable Polymer Networks Comprising Ester-Urethane Building Block, PEGylated Fibrinogen and Catechol Units

Gokhan Demirci[1], *Malwina J. Niedźwiedź*[1], *Magdalena Charęza*[2], *Radosław Drozd*[2], *Miroslawa El Fray*[1]*

[1] Department of Polymer and Biomaterials Science, Faculty of Chemical Technology and Engineering, West Pomeranian University of Technology in Szczecin, Al. Piastów 45, 70-311 Szczecin, Poland
[2] Department of Microbiology and Biotechnology, Faculty of Biotechnology and Animal Husbandry, West Pomeranian University of Technology in Szczecin, 45 Piastów Avenue, 71-311 Szczecin, Poland

Abstract

Hydrophobic telechelic macromonomers derived from vegetable oil (VO) comprising ester-urethane linkages can be successfully photopolymerized after functionalization with methacrylic termini. While featuring hydrophobicity, they can be combined with PEGylated fibrinogen and methacrylated catecholamine to balance hydrophobic-hydrophilic properties. In this work, we performed hydrolytic and enzymatic degradation studies of amphiphilic (hybrid) UV-cured polymer networks in the presence of lipase . The degradation process was monitored by assessing structural changes via Fourier transform infrared spectroscopy, determining water uptake and weight loss, and revealing changes in surface morphology by micro-computed tomography. Incorporation of hydrophilic components into

hydrophobic core contributed to accelerated degradation after 4 weeks due to better penetration of water molecules into the amphiphilic network as manifested by increased water uptake up to 50 wt.% and mass loss of 9 wt.%, respectively. We demonstrated that lipase is active towards ester bonds cleavage in amphiphilic hybrids. Importantly, polymer networks did not release acidic degradation products in an amount that could cause acidification of the medium. This study reveals that tailoring the molecular structure allows for customization of the susceptibility of cross-linked polymers to degradation, depending on the needs.

Keywords: dimerized-fatty acid, telechelic macromonomers, PEGylated fibrinogen, methacrylated L-DOPA, hydrolytic and enzymatic degradation, micro-computed tomography

Corresponding author: mirfray@zut.edu.pl

1. Introduction

In the past few decades, there has been increasing interest in developing environmentally friendly materials for various applications [1–3]. Among these, polymers have emerged as a prominent class of materials due to their unique properties [4–7]. Besides the other polymers, biodegradable ones have gained significant attention, particularly in the medical field, as they offer a sustainable and innovative solution to address various challenges in healthcare. The versatility and potential of biodegradable polymers arise from their adjustable properties, including mechanical strength, biocompatibility, and degradation time, which can be tailored to meet specific medical requirements [8–11].

The natural origin of the material, while contributing to its environmental friendliness, does not inherently guarantee fast degradation. The rate of degradation is intricately linked to various factors such as chemical structure of the material, number and type of functional groups as well as its hydrophilicity [12–14]. Skrobot *et. al.* presented degradation profile of a various macromonomers based on fatty acid derivative comprising ester, anhydride and urethane groups. These served for creating photocurable networks featuring diverse architectures of

telechelic macromers, consisting of long chain derivatives of fatty acids, primarily linoleic acid, with dihydroxy, dicarboxy or diamino functionalities [15]. These polymer networks were subjected to hydrolytic and enzymatic degradation studies. The highest hydrolytic degradation ratio at 37 °C was observed for the polymers containing anhydride bonds. However, since the primary ingredient is hydrophobic dilinoleic ester, the mass loss of most of the networks was low, for example, the mass of polyester-urethane network decreased only by 2 % after 7 weeks of hydrolytic degradation. An acceleration of mass loss was observed in the presence of the enzyme (lipase from *Pseudomonas cepacia*), where after 3 weeks, the mass losses was approaching 4% [16].These results clearly show that hydrophobic polymer networks based on fatty acid exhibited relatively slow degradation, which can be further tailored by incorporation of hydrophilic components.

The extensive exploration of polymers modification through the incorporation of hydrophilic, often biological molecules, to create composites and hybrids is widely explored due to ease way of tailoring final properties pivotal for biomedical applications. Biological molecules have diverse applications in the biomedical field, spanning from tissue engineering and drug delivery to wound healing and surgical procedures [9,17–21]. One noteworthy biological molecule utilized in these studies is fibrinogen that is a soluble glycoprotein present in blood plasma, plays a crucial role in the coagulation cascade, making it integral to processes such as wound healing and tissue regeneration [22–25]. Hybrid materials derived from this protein provide an optimal environment for cell adhesion, proliferation, and differentiation. This renders them well-suited for tissue repair and regeneration [26,27].

The structure of fibrinogen, with its diverse functional groups, allows for various modifications. For instance, PEGylation involves introducing polyethylene glycol (PEG) chains to fibrinogen, imparting several advantages to the resulting biomaterials. PEGylation enhances the stability and solubility of fibrinogen, reduces its immunogenicity, and prolongs its

circulation time, thereby improving its overall biocompatibility. Furthermore, PEGylation can facilitate the adjustment of fibrinogen's degradation rate by proteolytic enzymes occurring in body fluids and tissues. This capability enables the design of biocompatible carriers with the potential for controlled release kinetics of active compounds and tailored degradation profiles. [28,29] [30]. The introduction of PEGylated fibrinogen into the hybrid structure imparts enhanced biodegradation of biomaterials making them more suitable for a broad spectrum of medical applications [31].

Various biomolecules and their derivatives are being also used to enhance functionalities of biomaterials. An interesting example is 3,4-dihydroxyl-L-phenylalanine (L-DOPA) which is derivative an natural amino acid, L-tyrosine [32,33]. L-DOPA can be modified by methacrylic acid that provides a versatile platform for the synthesis of polymeric networks. The incorporation of methacrylated L-DOPA into injectable biomaterials results in enhanced cell adhesion, enables the encapsulation of active compounds, and facilitates the localized delivery of therapeutic agents [34]. While hybrids derived from natural proteins and a variety of organic polymers show great potential, their expanded applications depend mainly on biocompatibility assessment. A key attribute is their ability to biodegrade within a certain time frame. This attribute is of great importance, especially for the use of such hybrids as materials for tissue regeneration.

In this study, our objective was to elucidate the susceptibility to biodegradation of newly prepared hybrid polymer networks based on hydrophobic ester-urethane telechelic macromonomers, PEGylated fibrinogen, and methacrylated L-DOPA. We examined the chemical structure of the hybrid components of final polymer network, as well as we determined the parameters of hydrolytic and enzymatic degradation, such as changes in chemical structure, water uptake, mass loss, and the pH of the degradation medium. We also assessed physico-chemical properties of the final photocured materials as a function of the

degradation time. Additionally, the structural changes in the surface morphology during the degradation was investigated by micro-computed tomography.

2. Experimental Section

2.1. Materials

Dimer linoleic acid-based polyester polyol (Priplast 1838) was kindly provided by Cargill Bioindustrial (The Netherlands). Isophorone diisocyanate (98%) (IPDI), tris (2-carboxyethyl) phosphine hydrochloride (TCEP.HCl), urea, polyethylene glycol (PEG) (4 kDa), 2-hydroxyethylmethacrylate (97%) (HEMA) and silicagel were purchased from Merck KGaA (Germany). Phenotiazine (PTZ), acryloyl chloride, diethyl ether, triethylamine (TEA), methacryloyl chloride, cyanogen bromide (CNBr), glacial acetic acid and zinc (II) acetyloacetonate (ZnAc), dimethyl sulfoxide (DMSO) and 3,4-dihydroxyl-L-phenylalanine (L-DOPA) were purchased from Sigma Aldrich (Poznań, Poland). Photoinitiator Omnirad 2022 was purchased from IGM Resins (The Netherlands). Phosphate buffered saline (PBS) was purchased from Eurochem (Poland). Borax was purchased from Alfa Aesar (Germany). Ethyl acetate (EtOAc), sodium carbonate, magnesium sulfate and ethanol were purchased from Chempur (Poland). Fibrinogen was purchased from SEGENS (France). HEMA was used after distillation under reduced pressure; all other reagents were used as received.

2.2. Synthesis of the Amphiphilic Hybrid Components

2.2.1. Synthesis of Telechelic Ester-urethane Macromonomer (Component A)

The synthesis of telechelic macromonomers was performed in two steps based on our previous work [15], with a recent modification [35]. Briefly, in the first step, 25 g (0.013 mmol) of polyester polyol (Priplast 1838) was reacted with 6.5 ml (0.052 mmol) of IPDI using ZnAc catalyst (2 mol% calculated relative to the amount of polyester polyol). In the second step, 6 mg (0.03 mmol) of phenothiazine (a polymerization inhibitor), a second aliquot of a catalyst

(the same mol% as in the first step), and 6.6 ml (0.054 mmol) of 2-hydroxyethyl methacrylate (HEMA) were introduced, while protecting the reaction from light. The progress of the reaction was monitored by tracking the ratio between FT-IR absorbance at 2262 cm^{-1} (A_{2262}), corresponding to N=C=O vibration in isocyanate groups of IPDI, and at 1526 cm^{-1} (A_{1526}), corresponding to N-H bending vibrations of the formed urethane bonds. The product was then precipitated into a four-fold excess of ice-cold methanol three times, and any residual solvent was evaporated under reduced pressure at 50 °C. The obtained product was a transparent, highly viscous, sticky, yellowish liquid.

2.2.2. Synthesis of PEGylated Fibrinogen (Component B)

2.2.2.1. PEG Diacrylate Synthesis

PEG-diacrylate (PEGDA) was prepared from linear PEG with a molecular weight of 4 kDa. Briefly, acrylation of PEG-OH was carried out under argon by reacting a dichloromethane (DCM) solution of PEG-OH with acryloyl chloride and triethylamine at a molar ratio of 1-OH to 1.5-acryloyl chloride to 1.5-triethylamine (0.2 g PEG/ml DCM) (Figure 1). The final product was precipitated in ice-cold diethyl ether and dried under vacuum overnight.

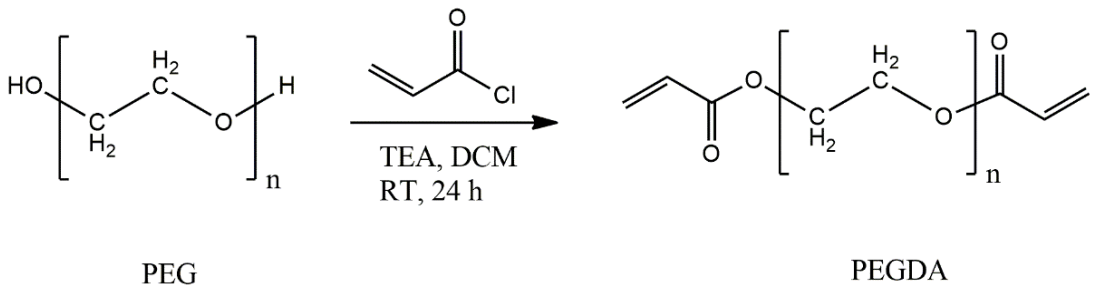

Figure 1 Reaction scheme of acrylation of polyethylene glycol

2.2.2.2.PEGylation of Fibrinogen

The following procedure was applied to PEGylate the protein: tris(2-carboxyethyl)phosphine hydrochloride (TCEP HCl) was added to a 7 mg/ml solution of fibrinogen in 50mM PBS with 8M urea (molar ratio 68:1 TCEP to fibrinogen cysteines). The solution was stirred for 15 minutes at 25 °C to fully dissolve. After dissolution, a solution of PEG-DA (250–300 mg/ml) in 50 mM PBS and 8 M urea was added and reacted overnight in the dark at 25 °C. The molar ratio of PEG to fibrinogen is 145:1 (linear PEG-DA, MW 4 kDa). The final PEGylated protein product was precipitated in a 5 fold excess of acetone at room temperature for 20 minutes while stirring. The precipitated protein solution was centrifuged for 20 minutes at 5000 rpm, and the obtained pellet was redissolved to a 20 mg/ml protein concentration in PBS containing 8 M urea. The PEGylated protein solution was then dialyzed against PBS containing 0.1% (v/v) glacial acetic acid at 4 °C for 2 days with twice-daily changes of PBS (Spectrum, 12–14 kDa MW cutoff). The lyophilized PEGylated fibrinogen was used right after lyophilization for creating the hybrids.

2.2.3. Synthesis of Methacrylated L-DOPA (Component C)

Synthesis of N-methacryloyl 3,4-dihydroxy-L-phenylalanine (L-DOPA) (Figure 2) was performed as follows: 1.15 g (5.69 mmol) of Borax was dissolved in 30 ml of water. The solution was degassed with argon for 30 minutes, after which 0.592 g (3.0 mmol) of L-DOPA was added and stirred for 15 minutes. Then, 0.317 g (3.0 mmol) of Na_2CO_3 was added, and the solution was cooled to 0 °C. Subsequently, 0.3 ml (3.0 mmol) of methacryloyl chloride was slowly added with stirring. The pH of the solution was maintained above 9 with Na_2CO_3 during the reaction. After stirring for 1 hour at room temperature, the solution was acidified to pH 2 with concentrated HCl. The mixture was extracted with ethyl acetate three times. After washing with 0.1 M HCl and drying over anhydrous $MgSO_4$, the solvent was removed in vacuo to yield a crude light brown solid. The product was further purified by elution from a silica gel column

with dichloromethane (DCM) and methanol (95:5). After evaporating the solvent, a white, sticky solid was obtained with a product yield of 35%.

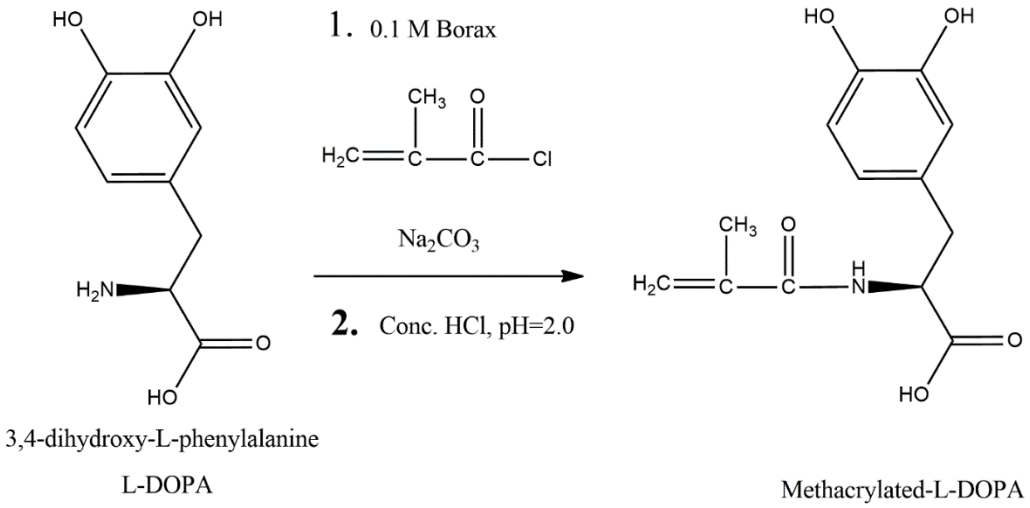

Figure 2 Reaction scheme of methacrylation of L-DOPA

2.3. Photocuring of the Hybrids

Photocured hybrid films were prepared according to the following procedure: approximately 20 g of macromonomer (component A) was dissolved, then various ratios of PEGylated fibrinogen (component B) and methacrylated L-DOPA (component C) were mixed homogeneously in an EtOAc:DMSO mixture (95:5 v/v%) in an amber flask. Hybrid A + B was prepared in ratio 90:10 wt%, while hybrid A + B + C in ratio: 85:5:10 wt%. Then, 1% w/w photoinitiator (Omnirad 2022) relative to the total amount of components was added to the mixture. Residual solvent was evaporated under reduced pressure after obtaining a homogeneous mixture. Subsequently, 1-mm-thick films were produced by pouring the final composition onto a glass plate and spreading it with a steel applicator. The composition was then irradiated with a DYMAX Bluewave LED Prime UVA light source (USA), with a narrow spectral range and maximum intensity at a wavelength (λ_{max}) of 385 nm. The intensity of the radiation was adjusted to 20 mW/cm^2 with the help of a radiometer, AktiPrint (Technigraf

GmbH). Photocuring was carried out under an argon atmosphere in a glove box. The exposure time was 150 seconds for each spot (2.25 cm^2) and was carried out stepwise across the entire plate (10 cm x 20 cm).

2.4. Characterization Methods

Fourier transform infrared spectroscopy (FTIR)

The FTIR was performed by using BRUKER ALPHA Platinum apparatus (Germany) at room temperature in the range of 4000–600 cm^{-1}, at a resolution of 2 cm^{-1} and using 32 scans. Liquid (viscous) macromonomer was analyzed in transmission mode, after pouring samples between NaCl plates. Spectra of films after photocuring and lyophilized PEGylated fibrinogen were obtained using reflection mode and the ATR snap-in with diamond crystal. Spectra were analyzed using EZ OMNIC software. Two-dimensional correlation spectroscopy (2D-COS) was used to obtain the sequence of individual spectral changes that resulted after the degradation.

Proton nuclear magnetic resonance (^{1}H NMR)

The NMR spectra of the macromonomer and methacrylated L-DOPA were recorded using Bruker DPX HD-400 MHz. The instrument was equipped with a 5 mm Z-gradient broadband decoupling inverse probe. All experiments were conducted at 25 °C. A and C samples for NMR were prepared by dissolving approx. 50 mg of macromonomer (A) in 0.7 ml of $CDCl_3$-*d* and 20 mg of methacrylated-L-DOPA (C) in 0.7 ml of DMSO-d_6.

Gel fraction of thin films

The gel fraction (GF) of the cross-linked polymer networks was assessed as a crucial parameter for evaluating their structural integrity. The samples were weighted ($W_{initial}$) and subjected to refluxing in a Soxhlet (Behr Labor-Technik, Germany) extraction apparatus utilizing ethyl acetate (EtOAc) as the solvent. Following refluxing, samples were dried under

reduced pressure until a constant mass (W_{final}) was achieved. The gel fraction was calculated according to following equation (1):

$$Gel\ fraction\ (\%) = \frac{W_{final}}{W_{initial}} * 100 \qquad (1)$$

The wettability of thin films

The wettability of thin films was evaluated with the use of the KRUSS DSA100 Drop Shape Analyzer. The tests were performed following the BS EN 828:2013 standard. The 2 μL droplet of distilled water was spotted on the sample. The camera incline and magnification were set to +1 degree and 7x, respectively. The laboratory temperature was 23.5 °C, and the drop fit method was "tangent 1". The results are averages of ten measurements, and the data presented were recorded after 3 s and 120 s.

Hydrolytic and enzymatic degradation

The biodegradation profile of the obtained amphiphilic hybrid networks was evaluated by performing hydrolytic and enzyme-catalyzed degradation. In the case of hydrolytic degradation, samples (disk diameter 1.2 cm cut using a manual puncher) were placed in 5 ml simulated body fluid (SBF) that was prepared in the laboratory and the pH was adjusted to 7.43 in a 12-well plate and then kept on a shaker in an incubator at 37 °C. Hydrolytic degradation was carried out for 7 weeks. Poly(ε-caprolactone) (PCL) (Capa 6430) was used as a positive control for hydrolytic and enzymatic degradation studies.

For assessment of materials susceptibility to enzymatic degradation, a microbial lipase from *Candida antarctica* was used (Sigma Aldrich, Germany). Samples were cut into 1 cm^2 square shapes and placed into a 5 mL Falcon tube. Next, 3.0 mL of lipase solution was added to the samples at a concentration of 25.0 U/ml. Sodium azide (POCh, Gliwice, Poland) was added to prevent the growth of bacteria. To maintain stable level of enzyme activity the solution was changed every 7 days up to 28 days.

The effect of SBF and lipase on hybrid networks was analyzed by measurement of water uptake and mass loss. Every week, samples were removed from the vials, flushed with deionized water, droplets were wiped with a cloth, and then weighed. Finally the samples were dried in the oven for 24 h at 50 °C, 60 mbar and weighted on analytical laboratory balance. Water uptake and mass loss were calculated according to the following equations.

Water uptake (P):

$$P = \frac{m_w - m_d}{m_d} * 100\% \qquad (2)$$

Mass loss (D):

$$D = \frac{m_0 - m_d}{m_0} * 100\% \qquad (3)$$

*m_0: weight before degradation

*m_w: weight of wet sample after degradation

*m_d: weight of dry sample after degradation

Surface morphology assessment

The micro-CT images reflecting surface topography were acquired from the samples subjected to hydrolytic and enzymatic degradation using a micro-computed tomography Bruker Skyscan 1272 (Germany). The acquisition parameters were configured as follows: current of 150 μA; voltage of 50 kV; frame averaging of 4; Cu 0.10 mm filter; pixel size of 2.25 μm; rotation of 360° with 0.1° step. After the acquisition, the reconstruction was performed using the software NRecon, version 1.7.0.4, with the Reconstruction engine InstaRecon, version 2.0.2.6.

3. Results and Discussion

3.1. *Chemical Structure of Macromonomer And PEGylated Fibrinogen by IR Spectroscopy*

FTIR spectroscopy offers advantages such as rapid data acquisition, high sensitivity, quantitative analysis capabilities, broad applicability to various sample types, and its utility in identifying functional groups and performing structural analysis. Therefore, FTIR spectroscopy was used to determine chemical structure the synthesized macromonomer and PEGylated fibrinogen. In the case of macromonomer, the FT-IR measurements confirmed that the chemical structure of the obtained material was consistent with the assumed reaction mechanism and with our recent work [35].

The chemical structure of the ester-urethane macromonomer (component A) assessed by ATR-FTIR spectra analysis confirmed terminal functionalization (methacrylation) as indicated by lack of the characteristic absorbance band of hydroxyl groups in the spectra (Figure 3) and the presence of the band at 1642 cm^{-1} and 940 cm^{-1} which correspond to stretching vibrations of C=C from the coupling of HEMA. The band at 3372 cm^{-1} correspond to H-bonding between N-H and the oxygen of the carbonyl group. The band around 1527 cm^{-1} is attributed to N-H bending and C-N stretching vibrations. The 1461 and 1419 cm^{-1} as well correspond to N-H bending vibrations. The band at approx. 1732 cm^{-1} is characteristic for stretching of C=O in ester bonds of the polyester polyol, urethane, and methacrylic groups. The ester related peaks are observed at 1303 and in the region from 1236-1046 $cm^{-1,}$ they are associated with the vibration of C-O-C , C-O and O-C-C. The bands in the range of 2858–2936 cm^{-1} and 1364 cm^{-1} have been assigned to C-H aliphatic stretching bands, representing the aliphatic chains of the soft segments.

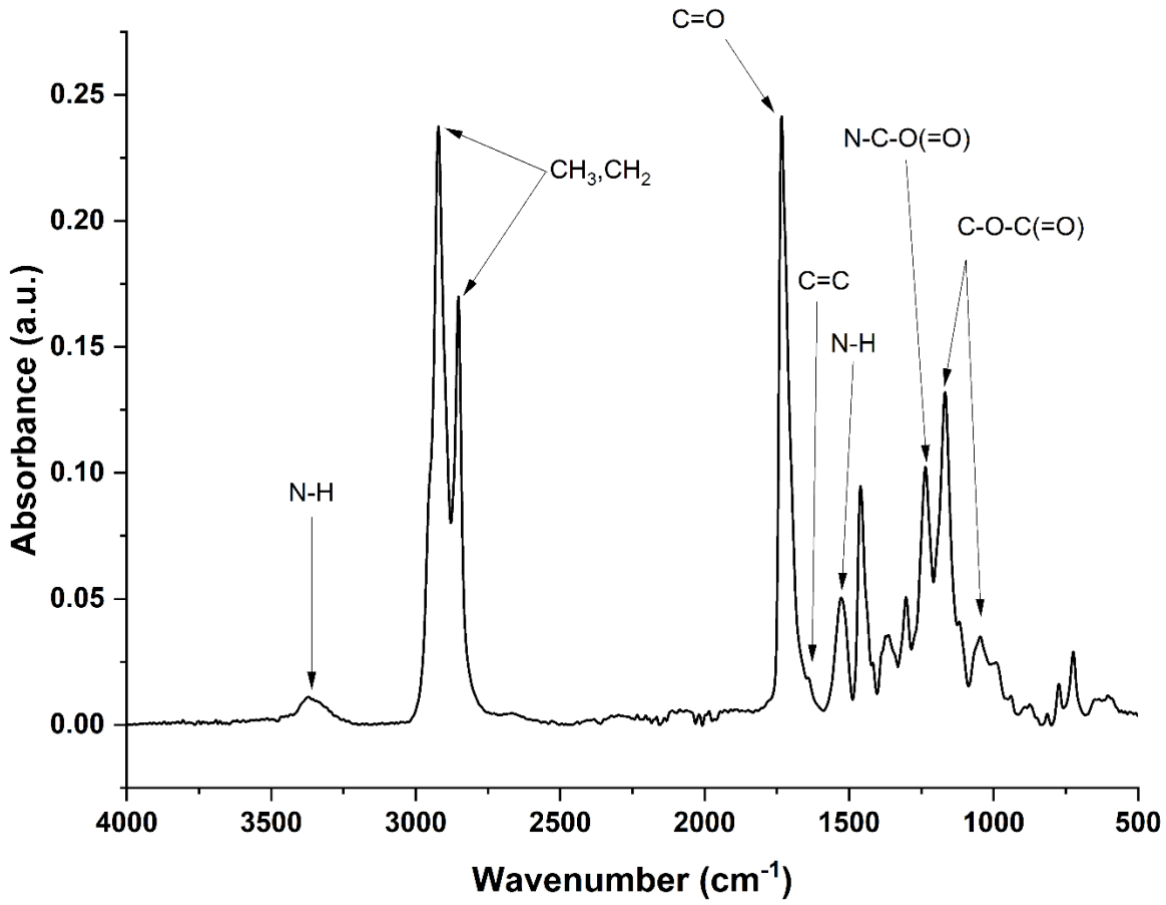

Figure 3 FT-IR spectrum of Component A

In the case of PEGylated fibrinogen, polyethylene glycol (PEG) is a polymer composed of repeating ethylene oxide units. The FT-IR spectroscopy (Figure 4) of PEGylated fibrinogen (component B) revealed characteristic bands in the region of 2800-3000 cm^{-1} which are associated with the stretching vibrations of the carbon-hydrogen bonds in the alkyl chain of polymer. The C-O stretching vibration is observed around 1359 cm^{-1} and 1279 cm^{-1}. A sharp peak around 1100-1300 cm^{-1} is attributed to the stretching vibration of the ether linkage (C-O-C) in the PEG backbone. The peak around the 1723 cm^{-1} corresponds to carbonyl group (C=O) and the band around 1636 cm^{-1} can be assign to vibration of aliphatic double bond (C=C) which confirmed successful synthesis of PEGDA. The bands at 1342 and 1100 cm^{-1} are due to C-H bending and C-O stretching vibration, respectively; and the band at 1242 cm^{-1} corresponds to C-H twisting vibrations. In the case of fibrinogen, the characteristic band is usually found in

the region of 1600-1700 cm^{-1} and arises from the C=O stretching vibration of the protein backbone, mainly from the amide bonds (C=O of the peptide bond). The band is typically observed around 1500-1580 cm^{-1} and originates from a combination of N-H bending and C-N stretching vibrations of the protein backbone. In the region of 1220-1300 cm^{-1}, a complex combination of C-N stretching, N-H bending, and C-C stretching vibrations of the protein backbone can be found.

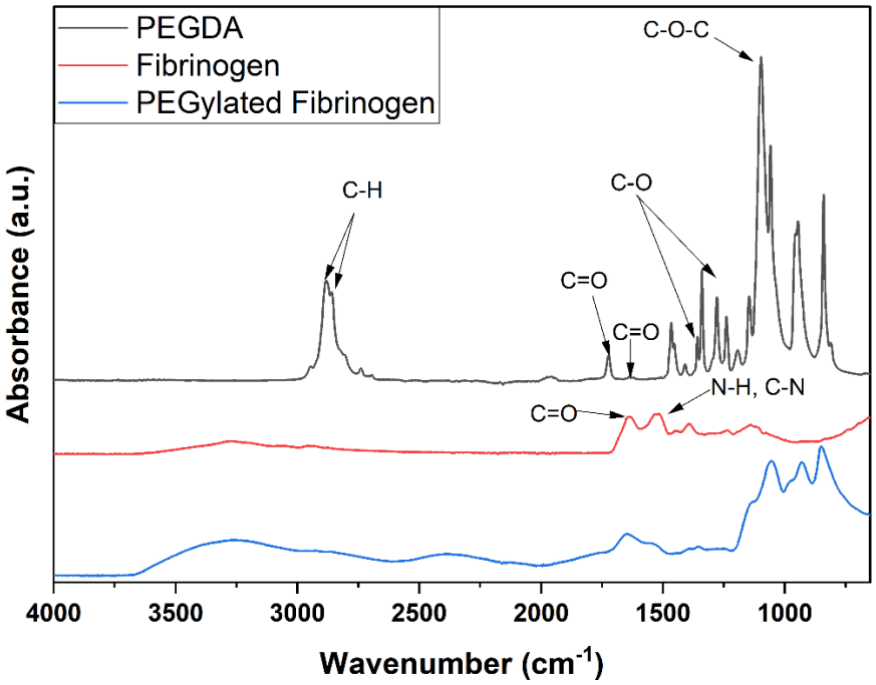

Figure 4 FT-IR spectra of blue: poly(ethylene glycol) diacrylate (PEGDA), red: PEGylated fibrinogen (component B), black: fibrinogen.

3.2 *Chemical Structure of Macromonomer and Methacrylated L-DOPA by NMR Spectroscopy*

NMR spectroscopy is favored for chemical structure analysis due to its non-destructive nature, information-rich spectra, quantitative capabilities, versatility in sample types, and its ability to provide detailed insights into molecular structures and dynamics. Therefore, the verification of chemical structure of synthetic components (A and C) of hybrid networks has

been performed using ^{1}H NMR spectroscopy. The analysis of NMR spectra also confirmed that the component A had a structure consistent with our expectations based on our prior work [35]. Figure 5a presents ^{1}H NMR spectra of a macromonomer that is used for the hybrids. In the ^{1}H-NMR spectrum, signals at 4.52 and 4.86 ppm confirm the presence of the NH groups of the urethane bonds, whereas signals at 5.61 and 6.16 ppm confirm the presence of C=C groups from the attachment of HEMA. In the case of methacrylated L-DOPA (component C) (Figure 5b), signal at 7.99 corresponds the N-H groups that has occurred during the methacrylation of L-DOPA. The other characteristic bonds are shown in the spectrum with their signals assignments.

a)

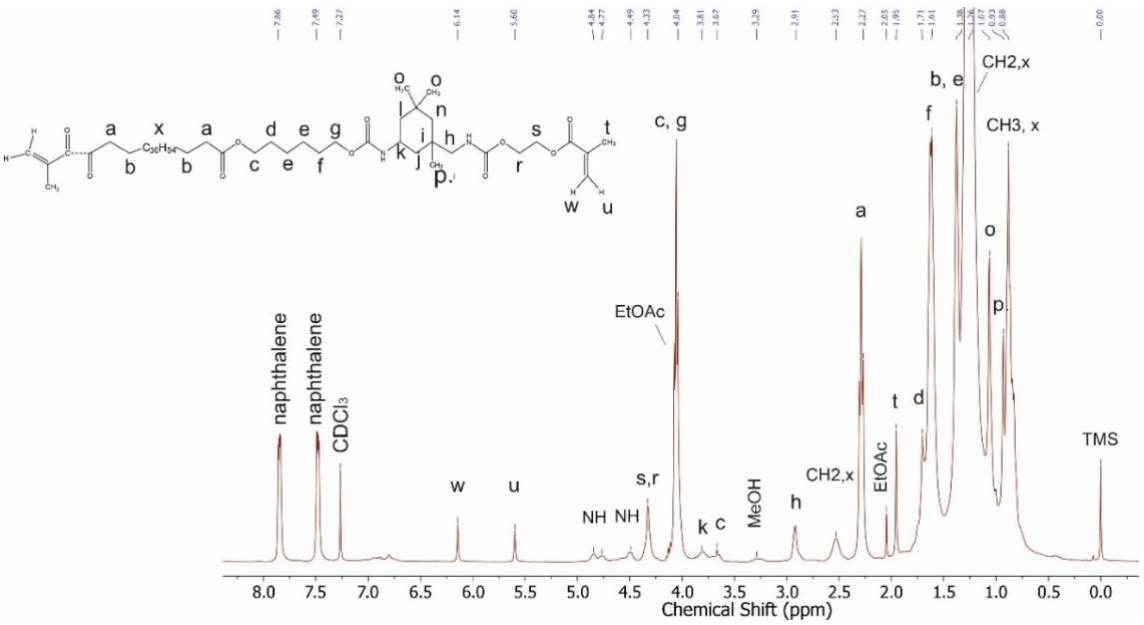

b)

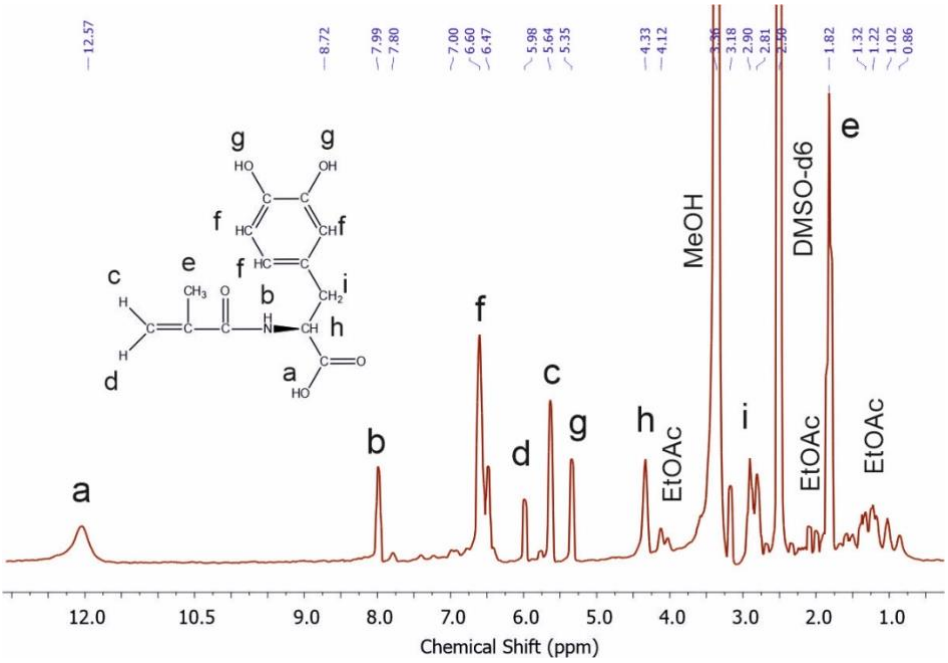

Figure 5 [1]H-NMR spectra of (a) macromonomer (component A) and (b) methacrylated L-DOPA (component C) with signals assignments.

3.3. *Gel Fraction of Thin Films*

The gel fractions of all photocured elastomers exceeded 80%, as illustrated in Figure 6. The highest results were obtained for polymer network containing only component A (91%). Slightly lower GFs, approximately 83%, were observed for hybrids, with no significant differences between A+B and A+B+C. The lower GF of hybrids in comparison to A can be assigned to incorporation of components B and C, respectively, which are easily swellable and degradable materials. Furthermore, it can be expected that the incorporation of B and C components will increase surface contact with water due to their polar nature, consequently accelerating its degradation.

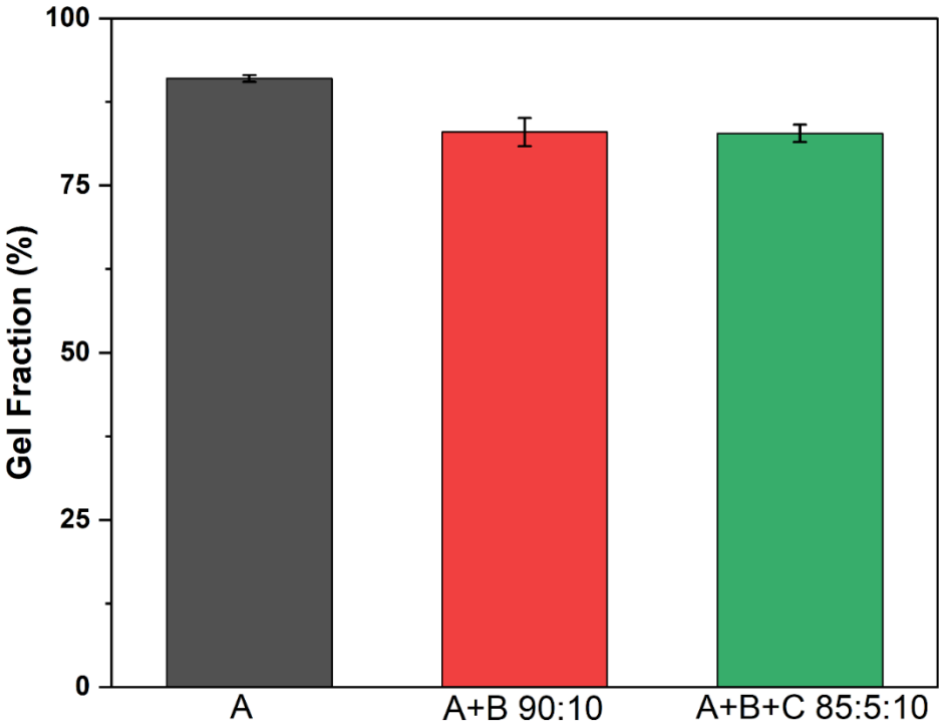

Figure 6 Gel fraction of photocured polymer networks

3.4. *Water Contact Angle of Photocured Hybrids*

The wettability of a biomaterial surface influences its interaction with biological entities, such as cells. Cells tend to adhere better to surfaces that exhibit suitable wettability, which is essential for promoting cell adhesion, spreading, and overall biocompatibility. Therefore, in order to assess the changes in surface wettability of photocured, multicomponent material comprising hydrophobic and hydrophilic building molecules, water contact angle measurements were performed. Since the materials were prepared on glass support, the surface which was in contact with air during photocuring has been assessed. The results are averages of ten measurements collected after 3 s and 120 s, respectively. The numerical values of average data are summarized in Table 1.

Table 1. Water contact angle values of the amphiphilic hybrids.

Samples	Contact time (seconds)		Water contact angle difference
	3	120	Δ
A	108.3±5.4	93.4±3.2	14.9
A+B 90:10	94.5±7.9	82.0±8.0	12.5
A+B+C 85:5:10	86.6±2.2	71.8±1.3	15.8

The water contact angle results revealed that the incorporation of PEGylated fibrinogen (component B) and methacrylated L-DOPA (component C) into hybrid system with macromonomer (component A) resulted in a greater reorganization of the structure of the material in contact with the air during the measurements. The macromonomer (component A), showed hydrophobic nature, due to the presence of fatty acid as a main component of this material. In the case of the hybrid A+B 90:10, the water contact angle decreased to 82.0 degree due to incorporation of PEGylated fibrinogen into the structure. The addition of L-DOPA (component C) further decreased, as expected, the surface hydrophilicity of photocured network to 71.8 degree (for A+B+C 85:5:10 network). This can be explained by presence of dihydroxy functionality of catechol within L-DOPA (Figure 2) which enables it to form strong hydrogen bonds with water [36]. Additionally, the aromatic ring participates in cation–π interactions with positively charged ions, a potent non-covalent interaction particularly effective in water.

3.4. *Biodegradation Studies*

Understanding the degradation profile of biomaterials is crucial for optimizing their performance and tailoring their application to specific clinical needs [29]. Degradation characteristics influence important parameters, including the release kinetics of encapsulated therapeutics, scaffold integrity, cellular behavior, and ultimately, tissue regeneration outcomes

[30]. Therefore, a comprehensive investigation into the degradation profiles of polymer hybrids containing hydrophobic macromonomer, and hydrophilic PEGylated fibrinogen and methacrylated L-DOPA is essential to uncover their full potential for biomedical applications.

3.5.1 Hydrolytic Degradation

Figures 7 a-c shows the FTIR spectra of the polymer hybrids while Figure 8 a-c shows the weight loss, water uptake and pH changes of crosslinked polymer networks after hydrolytic degradation.

a)

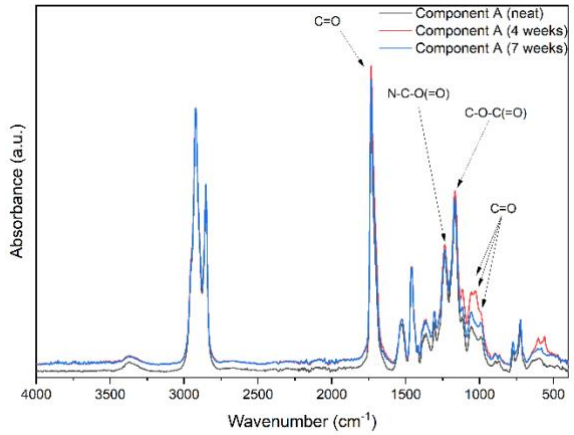

b)

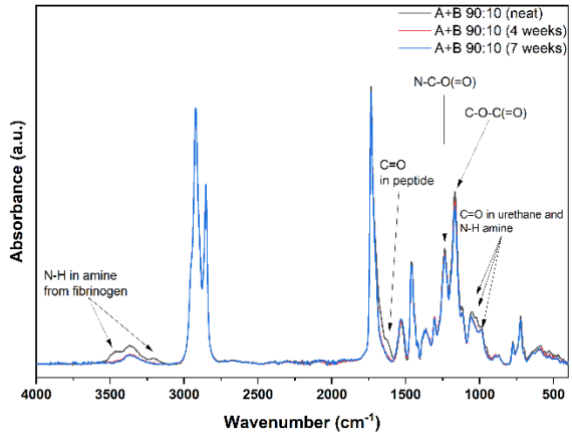

c)

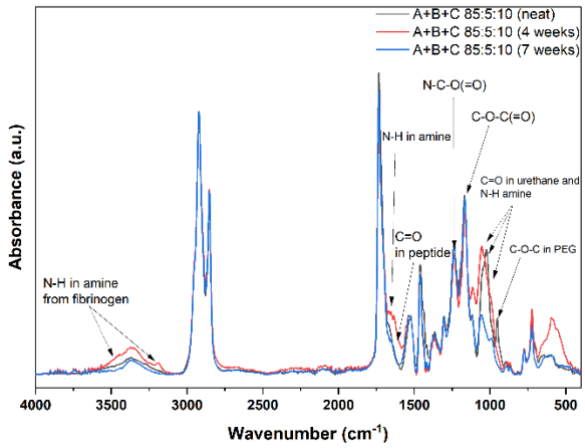

Figure 7 Changes in the chemical structure of polymer networks a) component A, b) component A + component B (90:10 wt.%) and c) component A+ component B+ component C (85:5:10 wt.%) during hydrolytic degradation

Infrared spectra of hydrophobic network comprising only component A (Figure 7a) before and after hydrolytic degradation revealed no significant differences, which may indicate a relative stability of the polymer structure. Noteworthy distinctions in peaks intensity are discernible within the spectral region from 1250 to 980 cm^{-1} where all observed peaks in the neat material are attributed to the vibration of the urethane functional groups bonds (like C-O, N-C(=O)-O, C-C-O, C-O-C). This outcome corroborates existing literature asserting the susceptibility of only selected functional groups to hydrolytic degradation, prominently including urethane bonds, which, upon hydrolysis, undergo decomposition to alcohol, amine and carbon dioxide. Moreover the bands corresponding to bending N-H vibration in aliphatic amines can be also well observed in the range from 1250 to 1020 cm^{-1}. Therefore, the differences observed in this region confirm the hydrolysis of polyurethane into amine. Additionally, the band at around 953 cm^{-1}, which is linked to the vibration of C-O-C in PEG, completely vanishes after 4 weeks. Incorporation of hydrophilic PEGylated fibrinogen (Figure 7b) revealed discernible variances within two regions at the FT-IR spectra, namely 3500-3200 cm^{-1} and 1637 cm^{-1}. The absence of a band at 1650cm^{-1} after 4 and 7 weeks of experiment suggest successful degradation of peptide bond. Furthermore, the disappearance of bands at 3212 and 3450 cm^{-1} attributed to the hydrogen bonding between the amine (-NH) and carbonyl (-C=O) groups of the peptide backbone, further corroborates this observation during degradation, aligning with previous statement. Incorporation of catechol units (Figure 6c) revealed significant differences in the range of 3500-3200 cm-^{1} indicative of the changes taking place in the ester and amide groups. The presence of bands at 1660 cm^{-1} and 1530 cm^{-1} might be attributed to -NH bending vibration of degradation product (primary and secondary amine).

Slight changes in chemical structure of investigated materials after hydrolytic degradation based on IR spectroscopy were also consistent with a slight weight loss (Figure 8 a) after 7 days which was observed for all the polymer networks (~2.5 wt.%). Such mas loss may be attributed to the uncross-linked top layer rapidly washed off from the polymer surface. The highest water absorption (Figure 8b) of approximately 10 wt.%. was observed for amphiphilic hybrid comprising 10 wt.% of PEGylated fibrinogen (component B). These results can be attributed to more hydrophilic nature of a hybrid after incorporating biomolecule. The slow hydrolytic degradation of the obtained hybrids closely correlates with the slight changes in the pH medium (Fig. 8c). Importantly, all materials (component A alone, and hybrids comprising PEGylated fibrinogen and component C, methacrylated L-DOPA) did not release acidic degradation products.

a)

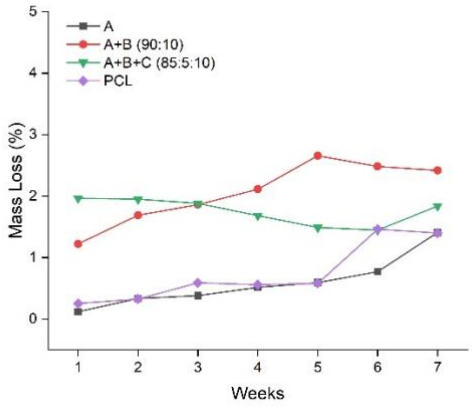

b)

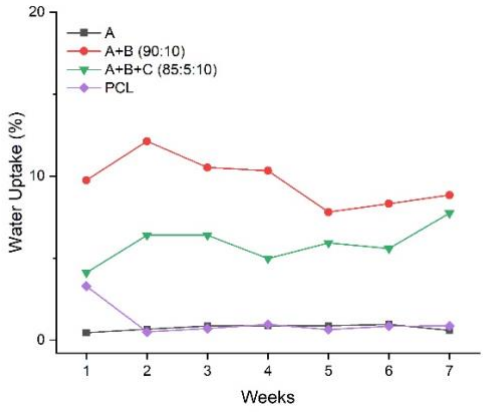

c)

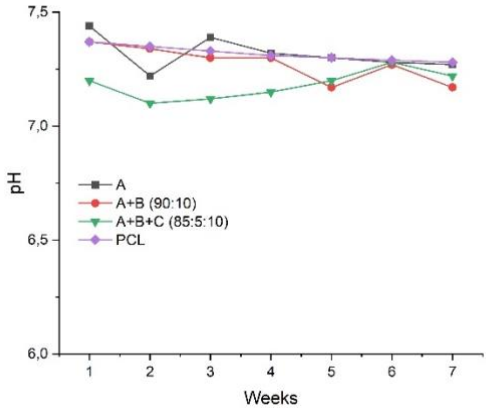

Figure 8 Mass loss a), water uptake b), and c) pH changes during hydrolytic degradation of photocured networks

3.5.2 Enzymatic Degradation

Figures 9a-c show the mass loss, water uptake, and pH changes of the photocured hybrid networks during enzymatic degradation catalyzed by lipase. Enzymatic degradation of PCL (reference material) and cross-linked polymer networks shows clear differences in their behavior as expressed by mass loss (Figure 9a). While the reference material is highly susceptible to degradation by lipase and has lost 100% of mass after two weeks, the mas loss of polymer network comprising component A reached only 2 wt.%, and hybrid network comprising component A and B revealed 4% mass loss. Incorporation of methacrylated L-DOPA into A and B components revealed 10 wt.% mass loss after 4 weeks. The water uptake (Figure 9b) of polymer networks increased from less than 1 wt.% to 3 wt.% after 4 weeks of degradation for component A. Incorporation of PEGylated fibrinogen into hydrophobic ester-urethane macromonomer showed 18 wt.% of water uptake while incorporation of methacrylated L-DOPA further increased water uptake to 50 wt.% after 4 weeks of enzymatic degradation. This constant increase in water absorption in the presence of lipase is most probably due to a decrease in network density of *in situ* photocured three-component network. Possible loosening of the network allows enzyme and water penetrate the structure. Performed gel fraction study

showed 10% difference between the hybrid and neat A component. Fibrinogen is well known to have low WCA with polar as well as non-polar solvents [37].

a) b)

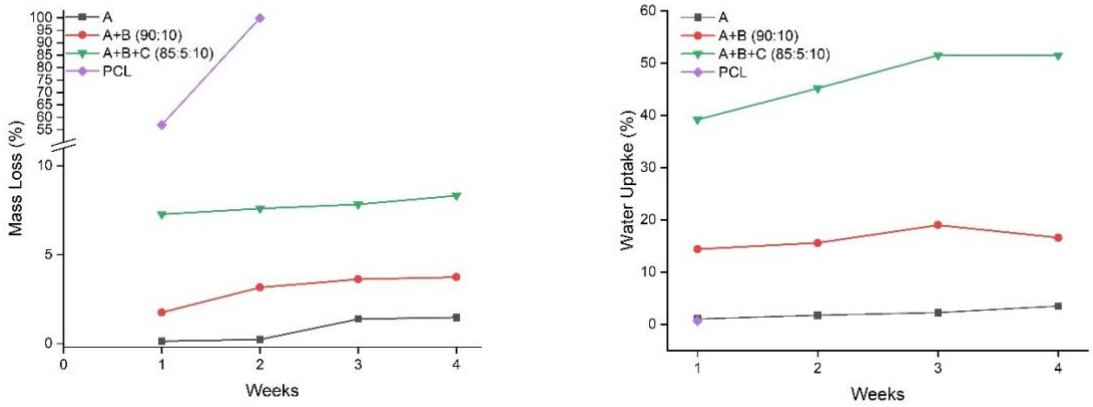

c)

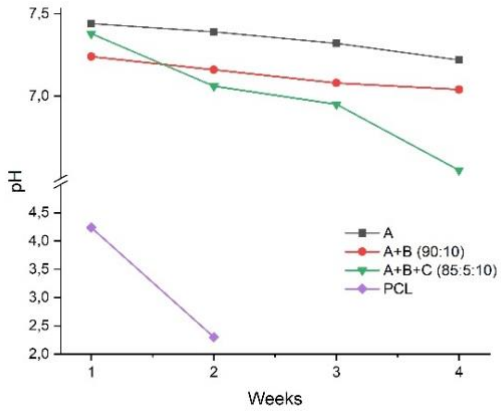

Figure 9 a) Mass loss, b) water uptake and c) pH changes during enzymatic degradation of photocured networks

The FTIR spectra of the polymer hybrids are presented in SI (Figure S1). However, in order to have deeper insights into the changes of polymer network structure during the degradation , the 2D-COS analysis of ATR-FTIR spectra has been performed.

The 2D-COS analysis of ATR-FTIR of the polymer network spectra (Figure 10) pointed out the degradation of the ester and urethane bond within component A by lipase action that

was indicated on synchronous spectra by set of autobands at 1733 cm^{-1}, 1551 cm^{-1}, 1451 cm^{-1} and 1413 cm^{-1}, 1177 cm^{-1} (Figure 10a).

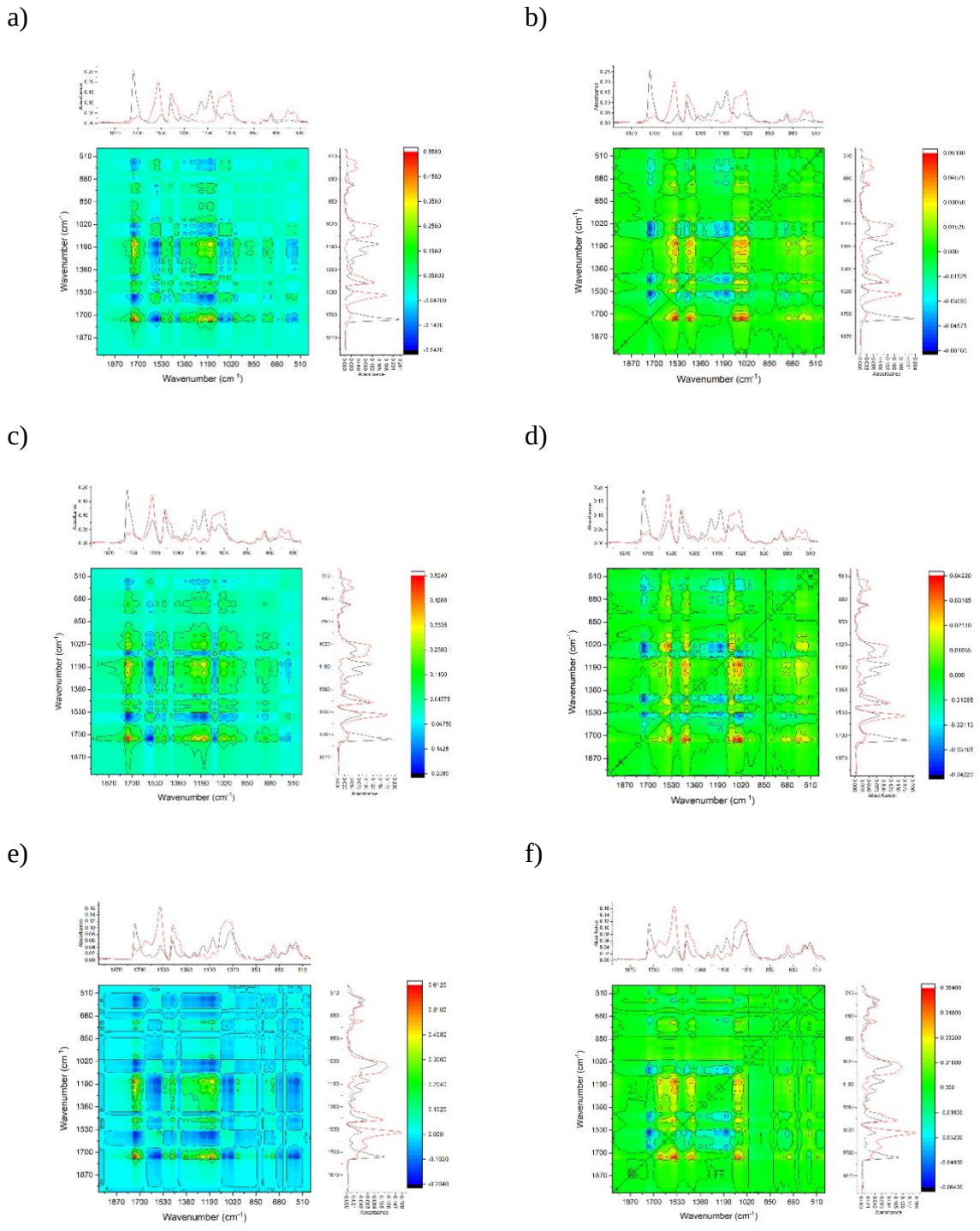

Figure 10 The 2D-COS analysis of ATR-FTIR spectra for; component A (a, b), component A+ component B (90:10 wt.%) (c,d), and component A+ component B+ component C (85:5:10

wt.%) (e, f). In the left column are synchronous plots, and in the right column are asynchronous plots. The colors on the bars indicate the strength and direction of correlations. The bands on the diagonal in synchronous plots indicate the autobands. The blue spots on synchronous plots indicate negative crossbands (negative correlation), while the spots with warm colors indicate positive crossbands.

The component A decomposition was indicated by intensive negative crossbands 1733 cm^{-1} vs 1551 cm^{-1}, 1451 cm^{-1}, 1413 cm^{-1} and 1177 cm^{-1}, that marked degradation of ester bonds and formation of -OH and COO^- groups. The same signal profile on 2D-COS spectra were observed for combination of component A and B and also C (Figure 10c-f). With the progress of degradation, the urethane band intensity increases in comparison with the intensity of the ester band, which proves that the degradation of the ester bonds and urethane bonds were relatively fast during the study. The main difference between analyzed samples was observed on synchronous spectra for component A + B where intensive negative crossbands 1733 cm^{-1} vs 1551 cm^{-1} (N-H bending and C-N stretching vibrations of the protein backbone), indicated on the exposed fibrinogen part of the hybrid.

3.5.4 Morphology of Polymer Structures by Micro-CT

The morphology changes of the polymer structures before/after hydrolytic and enzymatic degradation were observed by micro-computed tomography, and the results are presented in Figure 11. Additionally, the surface roughness changes in the structure of polymer networks before/after degradation of component A, component A + component B (90:10 wt.%) and component A + component B + component C (85:5:10 wt.%) are presented in Supplementary Information (see SI, Figure S2). As seen in Figure S2, the surface roughness increased in component A as well as in the hybrids especially after enzymatic degradation, due to the cleavage of ester bonds within the structure of component A, which constitutes the highest mass percentage of the hybrids. The increase in surface roughness was expected, as the

penetration of enzyme into the material contributed to this effect. According to the micro-CT images in Figure 11, the surface of the materials incubated in the SBF solution closely resembled the sample incubated without the enzyme. The analysis of surface morphology of the hybrids comprising hydrophobic macromonomer (component A) and hydrophilic PEGylated fibrinogen (component B) and the materials containing additionally methacrylated L-DOPA (component C) revealed a significant alteration of the surface morphology after exposure to lipase. The presence of enzyme triggered formation of pores with varying dimensions (in a range of 3-7 μm), with the largest being observed for networks comprising highest amount of component A bearing ester groups. Overall, the surface of the hybrids subjected to lipase treatment underwent substantial changes, characterized by the disruption of these regular pores and the emergence of wide cavities and irregular grooves. Such macroscopic roughness could be beneficial for larger cells, such as osteoblasts to promote better adhesion. It is worth noting that the neat samples A and A+B are relatively smooth thus indicating their potential in promoting neuronal cell response to nanoscale rough by increase of both the length of the axon and the number of branches of neurites.

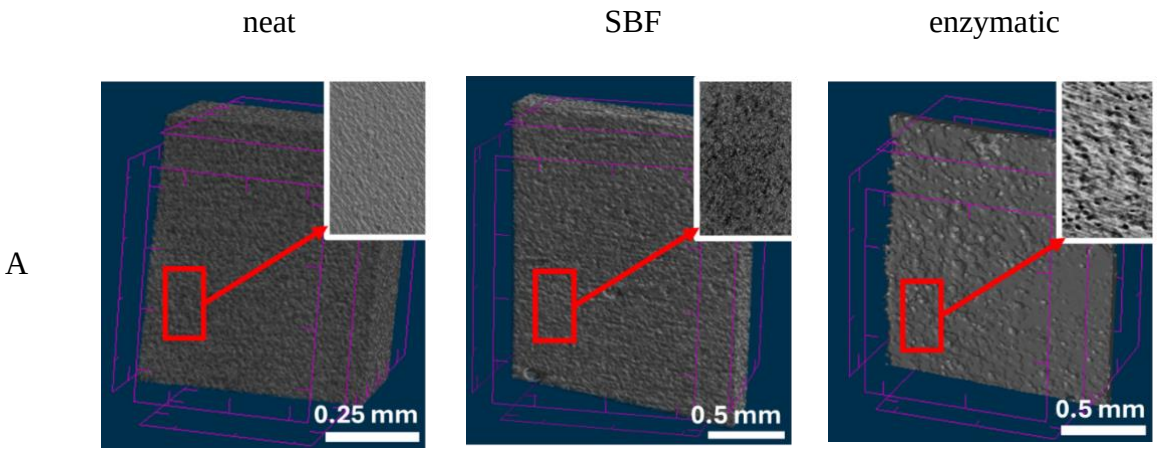

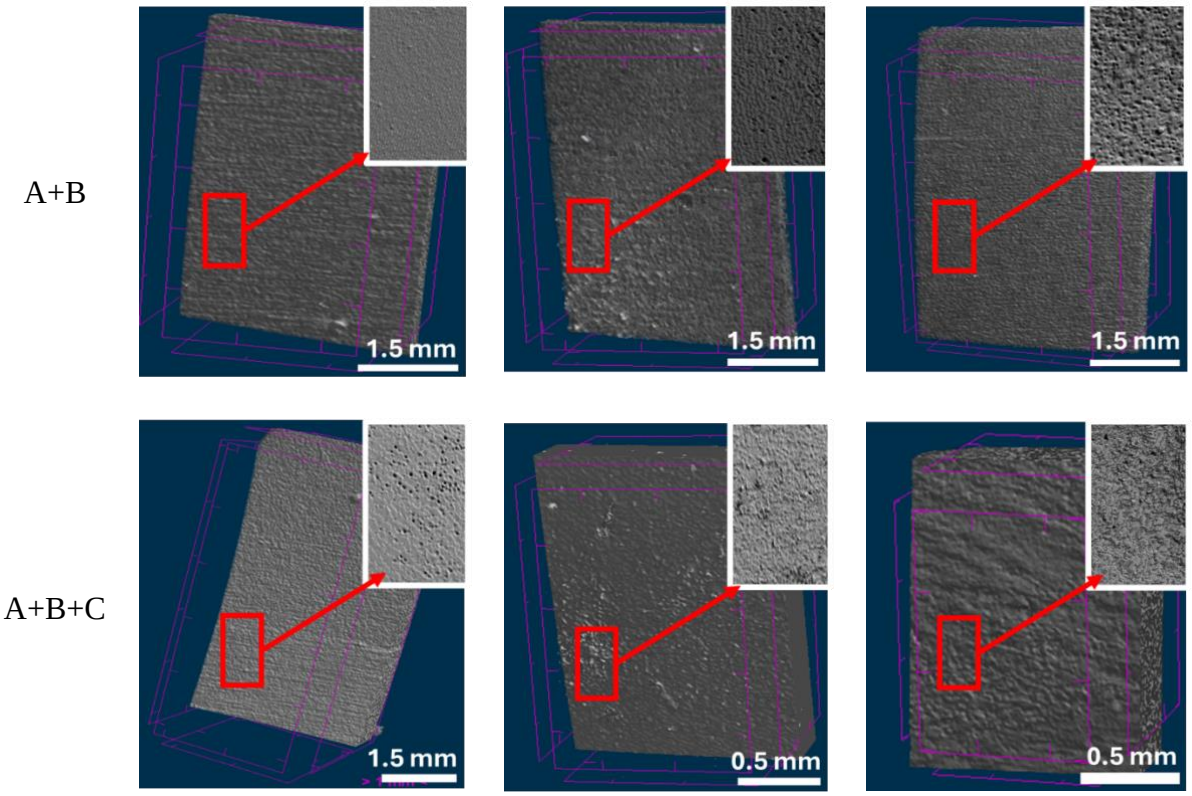

Figure 11 Morphology changes in the structure of polymer networks: a) neat, b) after hydrolytic and c) enzymatic degradation of component A; d) neat, c) after hydrolytic and d) enzymatic degradation of component A + component B (90:10 wt.%) and g) neat, h) after hydrolytic and i) enzymatic degradation of component A + component B + component C (85:5:10 wt.%)

4. Conclusions

In this study, the biodegradation process of flexible polymeric hybrids, fabricated using telechelic macromonomers, PEGylated fibrinogen, and methacrylated L-DOPA was investigated. Exploring the effect of SBF on newly designed hybrids demonstrated minor impact on the mass loss and water absorption, which remained relatively constant or increased very slightly after the first week of the incubation. The crosslinked hybrids showed no significant differences in pH changes of degradation medium, indicating no changes in the hybrid structure during hydrolytic degradation. Infrared analysis of the hybrids revealed the formation of new functional groups with terminal carboxylic and hydroxyl groups after

enzymatic degradation (in the presence of lipase) thereby confirming the cleavage of the ester groups. The degradation studies also revealed changes in the surface morphology of the polymer networks, particularly after enzymatic degradation. The increase in surface roughness, as observed in micro-CT images was attributed to the cleavage of ester bonds within component A. The exposure to lipase led to the formation of pores and substantial surface disruption in the hybrid materials, indicating the influence of enzymatic activity on structural integrity. All discussed results confirm the suitability of the considered flexible polymer networks for biomedical applications where controlled slow degradation and surface roughness is a desirable feature for specific cell type and size.

CRediT authorship contribution statement

Gokhan Demirci – investigation, conceptualization, data curation, methodology, writing – review & editing, **Malwina J. Niedźwiedź** – investigation, methodology, data curation, writing, **Magdalena Charęza–** investigation, **Radosław Drozd,** writing – review & editing, **Miroslawa El Fray** – conceptualization, supervision, writing – review & editing, funding acquisition.

Acknowledgements

This work was supported by research project OPUS17 from the Polish National Science Center (NCN) „Hybrid and elastomeric polymer networks: synthesis, structure and properties”; under Grant UMO-2019/33/B/ST5/01445. The authors thank Nina Stefaniak for assisting degradation studies.

5. References

[1] Tappa K, Jammalamadaka U. Novel Biomaterials Used in Medical 3D Printing Techniques. J Funct Biomater 2018;9:17. https://doi.org/10.3390/jfb9010017.

[2] Olbrich JM, Tate PL, Corbett JT, Lindsey JM, Nagatomi SD, Shalaby WSW, et al. Injectable in situ forming controlled release implant composed of a poly-ether-ester-carbonate and applications in the field of chemotherapy. J Biomed Mater Res - Part A 2012;100 A:2365–72. https://doi.org/10.1002/jbm.a.34179.

[3] Del Bakhshayesh AR, Asadi N, Alihemmati A, Tayefi Nasrabadi H, Montaseri A, Davaran S, et al. An overview of advanced biocompatible and biomimetic materials for creation of replacement structures in the musculoskeletal systems: focusing on cartilage tissue engineering. J Biol Eng 2019;13:85. https://doi.org/10.1186/s13036-019-0209-9.

[4] Li L, Yu F, Zheng L, Wang R, Yan W, Wang Z, et al. Natural hydrogels for cartilage regeneration: Modification, preparation and application. J Orthop Transl 2019;17:26–41. https://doi.org/10.1016/j.jot.2018.09.003.

[5] Chen Q, Liang S, Thouas GA. Elastomeric biomaterials for tissue engineering. Prog Polym Sci 2013;38:584–671. https://doi.org/10.1016/j.progpolymsci.2012.05.003.

[6] Vendamme R, Eevers W. Sticky Degradable Bioelastomers. Chem Mater 2017;29:5353–63. https://doi.org/10.1021/acs.chemmater.7b01635.

[7] Ulery BD, Nair LS, Laurencin CT. Biomedical applications of biodegradable polymers. J Polym Sci Part B Polym Phys 2011;49:832–64. https://doi.org/10.1002/polb.22259.

[8] Xu C, Okpokwasili C, Huang Y, Shi X, Wu J, Liao J, et al. Optimizing Anisotropic Polyurethane Scaffolds to Mechanically Match with Native Myocardium. ACS Biomater Sci Eng 2020;6:2757–69. https://doi.org/10.1021/acsbiomaterials.9b01860.

[9] Arun Y, Ghosh R, Domb AJ. Biodegradable Hydrophobic Injectable Polymers for Drug Delivery and Regenerative Medicine. Adv Funct Mater 2021;31:2010284.

https://doi.org/10.1002/adfm.202010284.

[10] Amsden B. Curable, biodegradable elastomers: emerging biomaterials for drug delivery and tissue engineering. Soft Matter 2007;3:1335. https://doi.org/10.1039/b707472g.

[11] Shi R, Chen D, Liu Q, Wu Y, Xu X, Zhang L, et al. Recent advances in synthetic bioelastomers. Int J Mol Sci 2009;10:4223–56. https://doi.org/10.3390/ijms10104223.

[12] Ghalia MA, Dahman Y. Advanced nanobiomaterials in tissue engineering. Nanobiomaterials Soft Tissue Eng., Elsevier; 2016, p. 141–72. https://doi.org/10.1016/B978-0-323-42865-1.00006-4.

[13] Silva RRA, Marques CS, Arruda TR, Teixeira SC, de Oliveira TV. Biodegradation of Polymers: Stages, Measurement, Standards and Prospects. Macromol 2023;3:371–99. https://doi.org/10.3390/macromol3020023.

[14] Vroman I, Tighzert L. Biodegradable Polymers. Materials (Basel) 2009;2:307–44. https://doi.org/10.3390/ma2020307.

[15] El Fray M, Skrobot J, Bolikal D, Kohn J. Synthesis and characterization of telechelic macromers containing fatty acid derivatives. React Funct Polym 2012;72:781–90. https://doi.org/10.1016/j.reactfunctpolym.2012.07.010.

[16] Skrobot J, Ignaczak W, El Fray M. Hydrolytic and enzymatic degradation of fl exible polymer networks comprising fatty acid derivatives. Polym Degrad Stab 2015;120:368–76. https://doi.org/10.1016/j.polymdegradstab.2015.07.022.

[17] Amsden BG. Biodegradable elastomers in drug delivery. Expert Opin Drug Deliv 2008;5:175–87. https://doi.org/10.1517/17425247.5.2.175.

[18] Sung YK, Kim SW. Recent advances in polymeric drug delivery systems. Biomater Res 2020;24:12. https://doi.org/10.1186/s40824-020-00190-7.

[19] Wen Q, Mithieux SM, Weiss AS. Elastin Biomaterials in Dermal Repair. Trends Biotechnol 2020;38:280–91. https://doi.org/10.1016/j.tibtech.2019.08.005.

[20] Litvinov RI, Weisel JW. Fibrin mechanical properties and their structural origins. Matrix Biol 2017;60–61:110–23. https://doi.org/10.1016/j.matbio.2016.08.003.

[21] Hejbøl EK, Sellathurai J, Nair PD, Schrøder HD. Injectable scaffold materials differ in their cell instructive effects on primary human myoblasts. J Tissue Eng 2017;8. https://doi.org/10.1177/2041731417717677.

[22] Pourshahrestani S, Zeimaran E, Kadri NA, Mutlu N, Boccaccini AR. Polymeric Hydrogel Systems as Emerging Biomaterial Platforms to Enable Hemostasis and Wound Healing. Adv Healthc Mater 2020;9:2000905. https://doi.org/10.1002/adhm.202000905.

[23] Li Y, Meng H, Liu Y, Lee BP. Fibrin Gel as an Injectable Biodegradable Scaffold and Cell Carrier for Tissue Engineering. Sci World J 2015;2015:1–10. https://doi.org/10.1155/2015/685690.

[24] Simaan-Yameen H, Bar-Am O, Saar G, Seliktar D. Methacrylated fibrinogen hydrogels for 3D cell culture and delivery. Acta Biomater 2023;164:94–110. https://doi.org/10.1016/j.actbio.2023.03.046.

[25] Jennewein C, Tran N, Paulus P, Ellinghaus P, Eble JA, Zacharowski K. Novel aspects of fibrin(ogen) fragments during inflammation. Mol Med 2011;17:568–73. https://doi.org/10.2119/molmed.2010.00146.

[26] Yu Z, Li H, Xia P, Kong W, Chang Y, Fu C, et al. Application of fibrin-based hydrogels for nerve protection and regeneration after spinal cord injury. J Biol Eng 2020;14:22. https://doi.org/10.1186/s13036-020-00244-3.

[27] Al Enezy-Ulbrich MA, Malyaran H, Lange RD, Labude N, Plum R, Rütten S, et al. Impact of Reactive Amphiphilic Copolymers on Mechanical Properties and Cell Responses of Fibrin-Based Hydrogels. Adv Funct Mater 2020;30:2003528. https://doi.org/10.1002/adfm.202003528.

[28] Gonen-Wadmany M, Goldshmid R, Seliktar D. Biological and mechanical implications of PEGylating proteins into hydrogel biomaterials. Biomaterials 2011;32:6025–33. https://doi.org/10.1016/j.biomaterials.2011.04.055.

[29] Oliveira MB, Kossover O, Mano JF, Seliktar D. Injectable PEGylated fibrinogen cell-laden microparticles made with a continuous solvent- and oil-free preparation method. Acta Biomater 2015;13:78–87. https://doi.org/10.1016/j.actbio.2014.11.013.

[30] Brown AC, Barker TH. Fibrin-based biomaterials: Modulation of macroscopic properties through rational design at the molecular level. Acta Biomater 2014;10:1502–14. https://doi.org/10.1016/j.actbio.2013.09.008.

[31] Deshayes S, Kasko AM. Polymeric biomaterials with engineered degradation. J Polym Sci Part A Polym Chem 2013;51:3531–66. https://doi.org/10.1002/pola.26765.

[32] Lee H, Scherer NF, Messersmith PB. Single-molecule mechanics of mussel adhesion. Proc Natl Acad Sci U S A 2006;103:12999–3003. https://doi.org/10.1073/pnas.0605552103.

[33] Moulay S. Dopa/Catechol-Tethered Polymers: Bioadhesives and Biomimetic Adhesive

Materials. Polym Rev 2014;54:436–513. https://doi.org/10.1080/15583724.2014.881373.

[34] Guvendiren M, Brass DA, Messersmith PB, Shull KR. Adhesion of DOPA-Functionalized Model Membranes to Hard and Soft Surfaces. J Adhes 2009;85:631–45. https://doi.org/10.1080/00218460902997000.

[35] Niedźwiedź MJ, Demirci G, Kantor-Malujdy N, Sobolewski P, El Fray M. Fatty-acid-derived ester-urethane macromonomers synthesized using bismuth and zinc catalysts. Eur Polym J 2022;170:111168. https://doi.org/10.1016/j.eurpolymj.2022.111168.

[36] Kord Forooshani P, Lee BP. Recent approaches in designing bioadhesive materials inspired by mussel adhesive protein. J Polym Sci Part A Polym Chem 2017;55:9–33. https://doi.org/10.1002/pola.28368.

[37] van Oss CJ. Surface properties of fibrinogen and fibrin. J Protein Chem 1990;9:487–91. https://doi.org/10.1007/BF01024625.